

# Biodegradable Nanofibrous Temperature-Responsive Gelling Microspheres for Heart Regeneration

Chao Zhao, Shuo Tian, Qihai Liu, Kemao Xiu, Jenglam Lei, Zhong Wang,\*  
and Peter X. Ma\*

Myocardial infarction (heart attack) is the number-one killer of heart patients. Existing treatments do not address cardiomyocyte (CM) loss and cannot regenerate the myocardium. Introducing exogenous cardiac cells is required for heart regeneration due to the lack of resident progenitor cells and very limited proliferative potential of adult CMs. Poor retention of transplanted cells is the critical bottleneck of heart regeneration. Here, the invention of a poly(l-lactic acid)-*b*-poly(ethylene glycol)-*b*-poly(N-Isopropylacrylamide) copolymer and its self-assembly into nanofibrous gelling microspheres (NF-GMS) is reported. The NF-GMS undergo a thermally responsive transition to form not only a 3D hydrogel after injection *in vivo*, but also exhibit characteristics mimicking the native extracellular matrix (ECM) of nanofibrous proteins and gelling proteoglycans or polysaccharides. By integrating the ECM-mimicking features, injectable form, and the capability of maintaining 3D geometry after injection, the transplantation of hESC-derived CMs carried by NF-GMS leads to a striking tenfold graft size increase over direct CM injection in rats, which is the highest reported engraftment to date. Furthermore, NF-GMS-carried CM transplantation dramatically reduces infarct size, enhances integration of transplanted CMs, stimulates vascularization in the infarct zone, and leads to a substantial recovery of cardiac function. The NF-GMS may also be utilized in a variety of biomedical applications.

## 1. Introduction


Cardiovascular disease is the leading cause of death in the world.<sup>[1]</sup> In particular, myocardial infarction (MI), commonly known as heart attack, results in permanent heart muscle damage or death, and is the number one killer of heart

patients. About 695 000 Americans suffer a new heart attack and about 325 000 Americans suffer a recurrent heart attack every year. A typical human heart attack causes the loss of approximately 1 billion cardiomyocytes (CMs). Patients who survive the heart attack often develop heart failure and sudden cardiac arrest due to severely weakened pumping function of the heart. Unfortunately, existing treatments for heart attack are primarily pharmacological or device-based, do not address the underlying problem of CM loss, cannot regenerate the myocardium, and cannot rescue the injured ventricle.<sup>[2]</sup> Indeed, the prevalence of chronic cardiomyopathy is steadily increasing.<sup>[3]</sup> Although re-entry of cell cycle is found in CMs after myocardial injury in adult mammalian heart, it does not lead to effective regeneration.<sup>[4]</sup> The outcome is age-dependent.<sup>[5]</sup> Recent studies show a lack of resident stem or progenitor cells in adult hearts that can regenerate the myocardium.<sup>[6]</sup> The introduction of exogenous CMs or their progenitor cells derived from pluripotent stem cells is a highly desired strategy for

heart regeneration because of their potential to regenerate the myocardium and restore the pumping function.<sup>[7]</sup> The Commonly used methods for cell transplantation include intravenous, intracoronary, and intramyocardial injections. Among them, intramyocardial injection directly delivers cells into the infarcted region, is more efficient, and is more

Dr. C. Zhao, Dr. Q. Liu, Dr. K. Xiu, Prof. P. X. Ma  
Department of Biologic and Materials Sciences  
University of Michigan  
Ann Arbor, MI 48109, USA  
E-mail: mapx@umich.edu

Dr. S. Tian, Dr. J. Lei, Prof. Z. Wang  
Department of Cardiac Surgery  
Frankel Cardiovascular Center  
University of Michigan  
Ann Arbor, MI 48109, USA  
E-mail: zhongw@umich.edu

 The ORCID identification number(s) for the author(s) of this article can be found under <https://doi.org/10.1002/adfm.202000776>.

DOI: 10.1002/adfm.202000776

Prof. P. X. Ma  
Department of Biomedical Engineering  
University of Michigan  
Ann Arbor, MI 48109, USA

Prof. P. X. Ma  
Macromolecular Science and Engineering Center  
University of Michigan  
Ann Arbor, MI 48109, USA

Prof. P. X. Ma  
Department of Materials Science and Engineering  
University of Michigan  
Ann Arbor, MI 48109, USA

widely used.<sup>[8]</sup> But even with intramyocardial injection, cell retention remains minimal (only about 2% of injected cells) and does not lead to efficient engraftment.<sup>[9]</sup> While various approaches including hydrogel delivery,<sup>[10]</sup> suturing,<sup>[11]</sup> engineered tissue patches, and survival-improving cocktails<sup>[12]</sup> have been explored, the efficiency of cell transplantation, functional integration, and subsequent maturation of transplanted CMs remain disappointing. One major challenge to heart regeneration is the harsh environment in the infarcted heart, which prevents either repopulation of endogenous CMs or/and retention and integration of transplanted CMs or their progenitor cells.

We hypothesize that an injectable cell carrier that mimics both the nanofibrous (NF) architecture of extracellular matrix (ECM) fibrillar proteins and the gelling property of extracellular proteoglycans or polysaccharides, will enable minimally invasive delivery of cells, enhance retention/integration, and provide regenerative microenvironment for cardiac regeneration and functional recovery. To address the critical challenge facing the field of heart regeneration, we successfully synthesized biodegradable poly(L-lactic acid)-*b*-poly(ethylene glycol)-*b*-poly(N-isopropyl acrylamide) (PLLA-PEG-PNIPAm) tri-block copolymers for the first time in this work and demonstrated that they could self-assemble into NF microspheres and in the presence of water could further form a hydrogel upon change from room temperature to body temperature. We termed this cell carrier nanofibrous gelling microspheres (NF-GMS) and examined the CM retention, engraftment, cardiac regeneration, and functional recovery.

## 2. Results

### 2.1. The Design and Synthesis of PLLA-PEG-PNIPAm Tri-Block Copolymers

The wounds in an infarcted heart are irregular in shape. Injectable carriers can be advantageous for minimally invasive cell delivery.<sup>[13]</sup> We designed the PLLA-PEG-PNIPAm tri-block copolymer based on the hypothesis that the PLLA block could be tailored to form NF microspheres, the PEG block could provide hydrophilicity to bind water and the PNIPAm block could become physical crosslinks to integrate these microspheres into a 3D hydrogel once delivered in vivo at the body temperature (Figure 1a).

The synthesis of amphiphilic ABC triblock copolymers is highly challenging due to the sharp contrast in polarity between these blocks.<sup>[14]</sup> Reversible addition-fragmentation chain transfer (RAFT) polymerization<sup>[15]</sup> and atom transfer radical polymerization (ATRP)<sup>[16]</sup> have been used to synthesize di-block and tri-block copolymers. However, for RAFT, a challenge is that a particular RAFT agent is only suitable for a limited set of monomers, but often not suitable for the subsequent two monomers<sup>[15a]</sup> in the case of triblock copolymer synthesis. For ATRP, termination and other side reactions occur in each step and are more prominent in multi-step ATRP reactions, resulting in less controlled structure of the aimed tri-block copolymers.<sup>[17]</sup> With the above considerations, we took a new approach, that is, ATRP and ROP (ring-opening

polymerization) two-step polymerization to synthesize the aimed PLLA-PEG-PNIPAm triblock copolymers, utilizing an asymmetric bifunctional macromolecular initiator, Br-PEG-OH. ATRP of NIPAm and the ROP of L-lactide are combined because the two types of polymerization are fully orthogonal (do not interfere with one another).<sup>[16,18]</sup> The presence of both the bromine end group and the hydroxyl end group of Br-PEG-OH ensures fast initiation of both ATRP and ROP. The synthesis of PLLA-PEG-PNIPAm copolymer was carried out in three steps (Figure 1b). First, Br-PEG-OH was synthesized using the reaction of bromoisobutyryl bromide (BIBB) with equimolar amount of anhydrous HO-PEG-OH in the presence of triethylamine (Et<sub>3</sub>N) according to the literature.<sup>[19]</sup> Second, hydroxyl-terminated diblock copolymer HO-PEG-PNIPAm was synthesized by ATRP of NIPAm monomer initiated by the bromine end group of Br-PEG-OH. Third, PLLA-PEG-PNIPAm triblock copolymer was synthesized by ROP of L-lactide initiated using the hydroxyl end group of HO-PEG-PNIPAm. With the above new approach, we successfully developed a reliable synthesis route for PLLA-PEG-PNIPAm triblock copolymers (Figures S1 and S2, Tables S1–S3, Supporting Information).

### 2.2. Thermo-Responsive Properties

By carefully examining the thermal responsive hydrodynamic diameter (D<sub>h</sub>) changes of the diblock PEG-PNIPAm and triblock PLLA-PEG-PNIPAm copolymers, we confirmed that the PNIPAm block in the triblock PLLA-PEG-PNIPAm copolymer underwent a rapid hydrophilic-hydrophobic transition to serve the aimed physical crosslinking function for hydrogel formation upon change from room temperature to body temperature (Figure S3, Supporting Information).

### 2.3. PLLA-PEG-PNIPAm NF-GMS Fabrication

PLLA-PEG-PNIPAm NF-GMS were fabricated through two-step self-assembling procedures (Figure 2a). First, the polymer was dissolved in tetrahydrofuran (THF) and emulsified into micro-scale liquid spheres in glycerol under rigorous stirring. The mixture was then quenched in liquid nitrogen to induce nano-scale phase separation for nanofiber formation. Next, the NF microspheres were obtained after solvent extraction with distilled water and freeze-drying. To achieve the NF feature, PLLA-PEG-PNIPAm triblock copolymers with varying compositions were synthesized for microsphere fabrication. When a PLLA-PEG-PNIPAm<sup>a</sup> copolymer was synthesized with a PEG block of a number average molecular weight ( $M_n$ ) of about 1550 (the unit for all molecular weights is g mol<sup>-1</sup>), a PNIPAm block of about 3800, and a PLLA block of about 1000, the fabricated microspheres had a smooth surface instead of an NF structure (Figure 2b). The failure to achieve the NF feature was attributed to short chain length of the PLLA. By controlling the PEG-PNIPAm/L-lactide ratio in the ROP of L-lactide, PLLA-PEG-PNIPAm<sup>b</sup> with the identical PEG ( $M_n = \approx 1550$ ) and PNIPAm ( $M_n = \approx 3800$ ) lengths but a longer PLLA length ( $M_n = \approx 2700$ ), microspheres with a platelet-like morphology

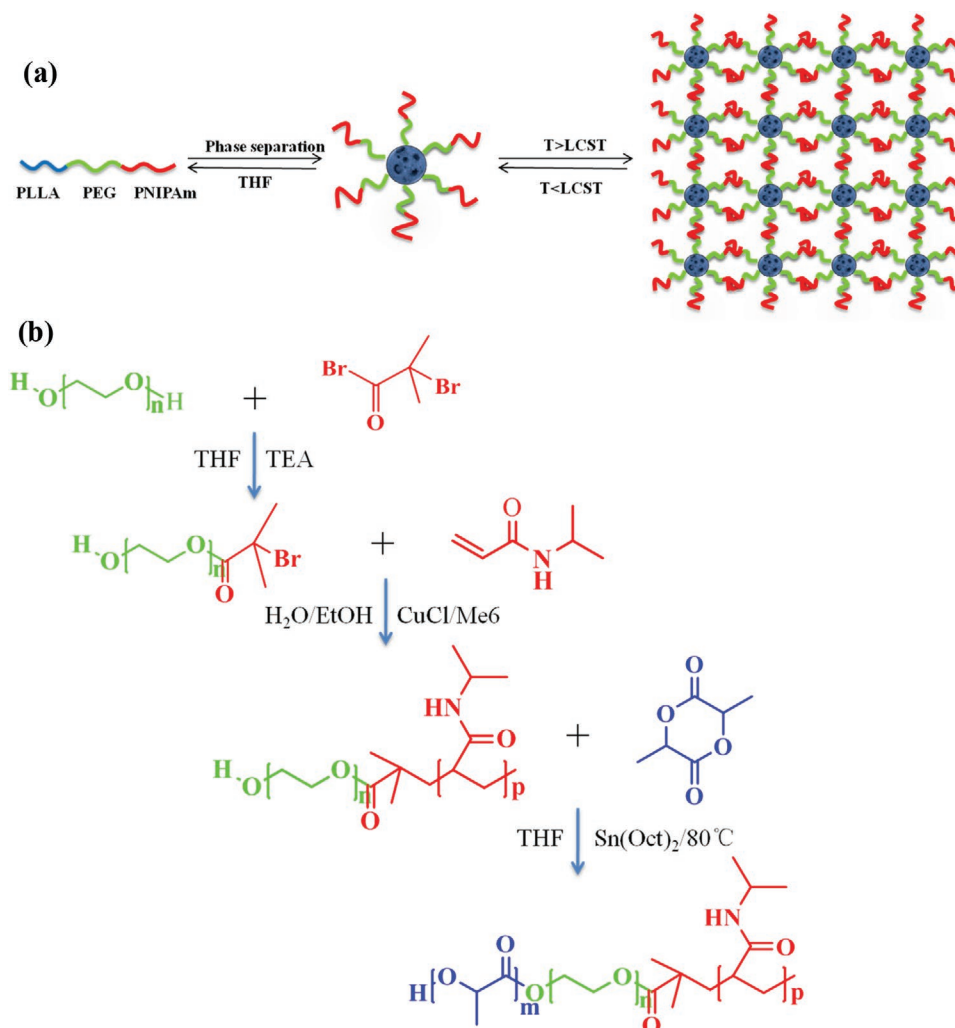


**Figure 1.** Triblock PLLA-PEG-PNIPAm copolymers and nanofibrous gelling microspheres (NF-GMS): a) A schematic of PLLA-PEG-PNIPAm triblock copolymer, its self-assembly into NF-GMS, and thermally induced physical crosslinking into hydrogel. b) A schematic of PLLA-PEG-PNIPAm triblock copolymer synthesis, which involves synthesis of double-headed PEG initiator, ATRP of NIPAm monomer, and ROP of L-lactide.

were formed (Figure 2c). When the  $M_n$  of PLLA block was further increased to  $\approx 11\,300$  (PLLA-PEG-PNIPAm<sup>c</sup>), microspheres with a typical NF structure were achieved (Figure 2d). The average diameter of the nanofibers in the microspheres was  $\approx 150$  nm, similar to those of ECM nanofibers. When the microsphere diameter reached, 30  $\mu\text{m}$  or greater, one or multiple holes formed in the nanofibrous microspheres (Figure S4, Supporting Information).

To visualize PLLA, PNIPAm, and PEG blocks in PLLA-PEG-PNIPAm NF-GMS, each of them was “chemically stained” with fluorescent monomer individually: Nile blue acrylamide (blue) was copolymerized into PLLA block, fluorescein *o*-acrylate (green) was copolymerized into PEG block, and acryloxyethyl thiocarbonyl rhodamine B (red) was copolymerized into PNIPAm block (see detailed methods in Supporting Information). As shown in Figure 3a, all of the three colors distributed throughout the microspheres. However, when observed at a higher magnification using a high-resolution confocal fluorescence microscope

(Leica SP8), PLLA blocks (blue) were observed to form a typical nanofibrous structure with more defined lines and dots (cross sections of nanofibers, high mag images in Figure 3a), while both PEG (green) and PNIPAm (red) blocks formed diffusive cloud-like structures surrounding the nanofibers. This observation was more obvious when the PLLA block fluorescent micrograph and PNIPAm or PEG block fluorescent micrographs were merged, where the PLLA fibers (blue) were surrounded by PNIPAm (red) or PEG (green) clouds, respectively (Figure 3a5,a6). These results suggested that self-assembled PLLA nanofibers with a fiber core-corona structure were formed in the NF-GMS, where PEG and PNIPAm blocks became the surrounding corona (Figure 3b).

The degradation property of a microcarrier is an important feature for consideration in tissue regeneration.<sup>[20]</sup> The PLLA-PEG-PNIPAm<sup>c</sup> NF-GMS disintegrated entirely into small pieces with about 50% weight loss after 8 weeks and about 70% weight loss after 15 weeks of incubation in PBS, whereas PLLA NF microspheres (with equivalent molecular weight)

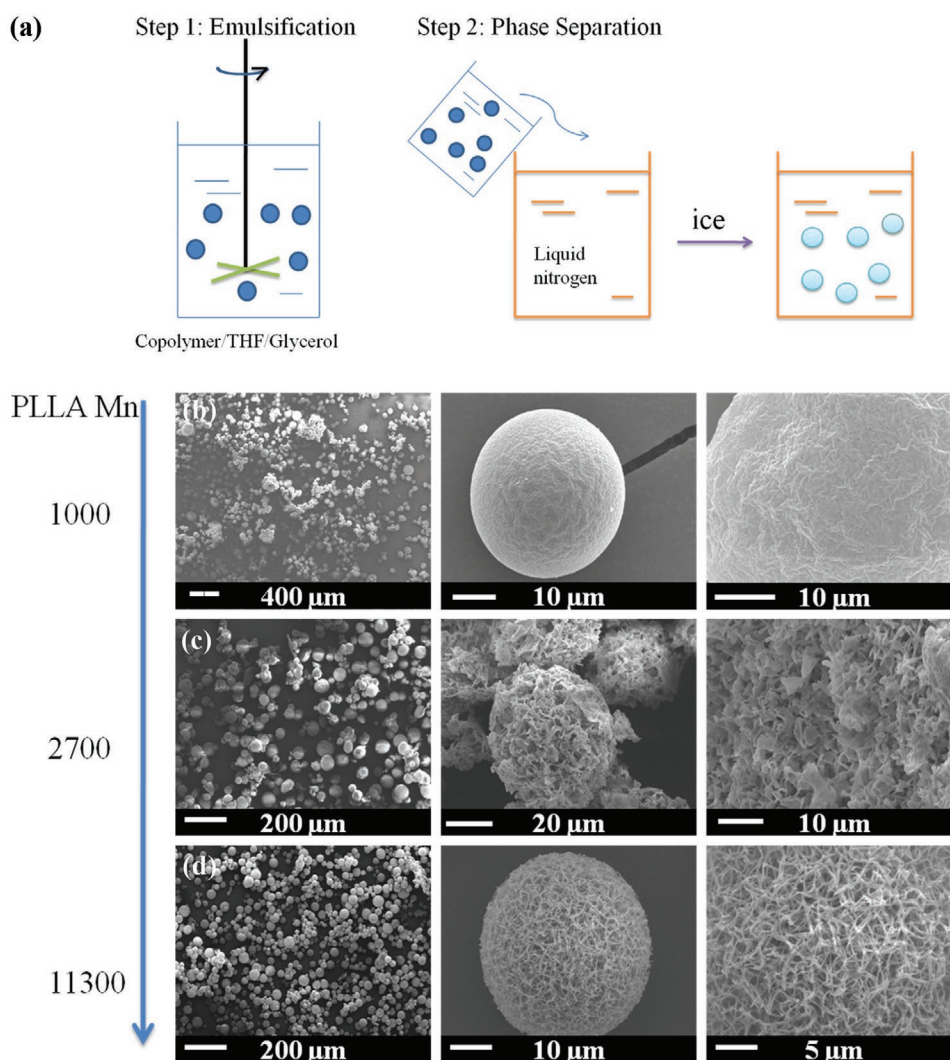


**Figure 2.** Molecular weight effect on nanofiber formation of PLLA-PEG-PNIPAm microspheres. a) A schematic of PLLA-PEG-PNIPAm microsphere fabrication. SEM micrographs of representative microspheres (30–60  $\mu\text{m}$ ) fabricated from b) PLLA-PEG-PNIPAm<sup>a</sup> (Table 1,  $M_n \approx 6376$ ), c) PLLA-PEG-PNIPAm<sup>b</sup> ( $M_n \approx 8042$ ), d) PLLA-PEG-PNIPAm<sup>c</sup> ( $M_n \approx 16665$ ).

remained intact with only about 10% weight loss after 15 weeks (Figures S5 and S6, Supporting Information), likely due to the substantial difference in hydrophilicity.

#### 2.4. Gelation Property of PLLA-PEG-PNIPAm NF-GMS

The novel PLLA-PEG-PNIPAm triblock copolymers with PLLA and PNIPAm as terminal blocks and PEG as the middle block were designed to assemble into nanofibrous microspheres that subsequently form a hydrogel (NF-GMS) upon temperature change from room temperature to body temperature. We selected a NF-GMS diameter range of 60–90  $\mu\text{m}$  (based on SEM observation) for subsequent cell transplantation studies. The size distribution was further measured using a Beckman Coulter Multisizer 4 (Figure S7, Supporting Information). At room temperature (25  $^{\circ}\text{C}$ ), the PLLA-PEG-PNIPAm<sup>c</sup> microspheres were a free-flowing liquid

(Figure 4a), whereas at the body temperature (37  $^{\circ}\text{C}$ ), they formed a 3D hydrogel (Figure 4b). However, the control two-block copolymers either remained a liquid suspension without PNIPAm (Figure 4c) or precipitated out without PEG (Figure 4d). The random copolymer of these three components could not form hydrogel either (Figure 4e), showing the requirement of the tri-block structure for the hydrogel formation.

The microstructure of PLLA-PEG-PNIPAm NF-GMS (60–90  $\mu\text{m}$ , 5 w/v% concentration, stained with rhodamine-BSA) was observed on a heated glass slide using confocal laser scanning microscopy. NF-GMS remained microspheres inside the formed 3D hydrogel (Figure 4f–h). The NF-GMS were able to stably maintain the 3D shape at 37  $^{\circ}\text{C}$  (Figure 4i) but not at 25  $^{\circ}\text{C}$  (Figure 4j). The PLLA nanofibrous hollow microspheres (NF-HMS) precipitated without hydrogel formation at 37  $^{\circ}\text{C}$  (Figure 4k), showing the requirement of water-binding PEG and physical crosslink-forming PNIPAm<sup>c</sup> at body temperature.

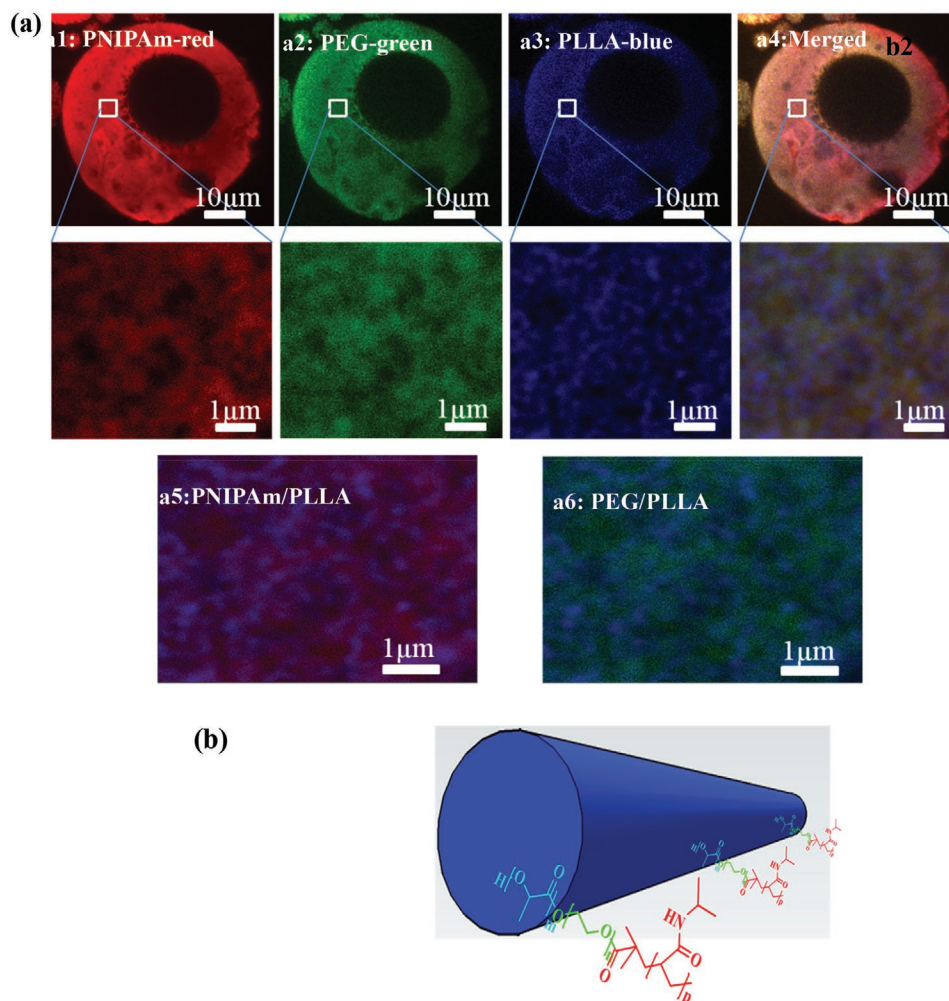


**Figure 3.** Confocal fluorescence micrographs of NF-GMS fabricated from PLLA-PEG-PNIPAm. a) 2D cross-sectional confocal fluorescence micrographs of NF-GMS fabricated from PLLA-PEG-PNIPAm<sup>c</sup> (60–90 μm based on SEM/confocal microscopy observation): a1) The PNIPAm blocks were stained by acryloyl ethyl thiocarbonyl rhodamine B (red), a2) the PEG blocks were stained by fluorescein *o*-acrylate (green), a3) the PLLA blocks were stained by Nile blue acrylamide (blue), a4) a merged fluorescence micrograph of three blocks. a5) A merged fluorescence micrograph of PNIPAm and PLLA blocks, a6) a merged fluorescence micrograph of PEG and PLLA blocks. b) A schematic of a nanofiber in the PLLA-PEG-PNIPAm NF-GMS with a core-corona structure.

Rheological studies were carried out to measure the sol–gel transition temperature and viscoelastic properties of NF-GMS (Section S5 and Figure S8, Supporting Information). The results confirmed that the aqueous suspension of PLLA-PEG-PNIPAm NF-GMS was a liquid at room temperature and became a free-standing hydrogel at body temperature. This hydrogel was shear-thinning, injectable, and its storage modulus could be modulated over more than two orders of magnitude at the body temperature by varying the composition and the polymer concentration.

### 2.5. Effect of PLLA-PEG-PNIPAm Composition on NF Structure and Gelation of NF-GMS

To systematically investigate the effect of PLLA-PEG-PNIPAm composition on the nanofibrous feature and gelation property

of NF-GMS, a library of PLLA-PEG-PNIPAm triblock copolymers with varying PEG, PNIPAm, and PLLA block lengths (Tables S1 and S2, Supporting Information), and linear PLLA homopolymers with three different molecular weights (Table S3, Supporting Information) were synthesized and fabricated into microspheres. The nanofibrous structure and gelation property of these microspheres were carefully evaluated (Section S6, Figure S9, and Table S1, Supporting Information). It was found that the nanofibrous structure and the gelation property of NF-GMS strongly depended on the composition of PLLA-PEG-PNIPAm copolymer. Two threshold requirements should be met simultaneously for the nanofiber formation (PLLA block molecular weight and its percentage) and two additional threshold requirements should be met simultaneously for the hydrogel formation (PEG and PNIPAm percentages). Only when the Mn of PLLA block was higher than about 5521, and the weight

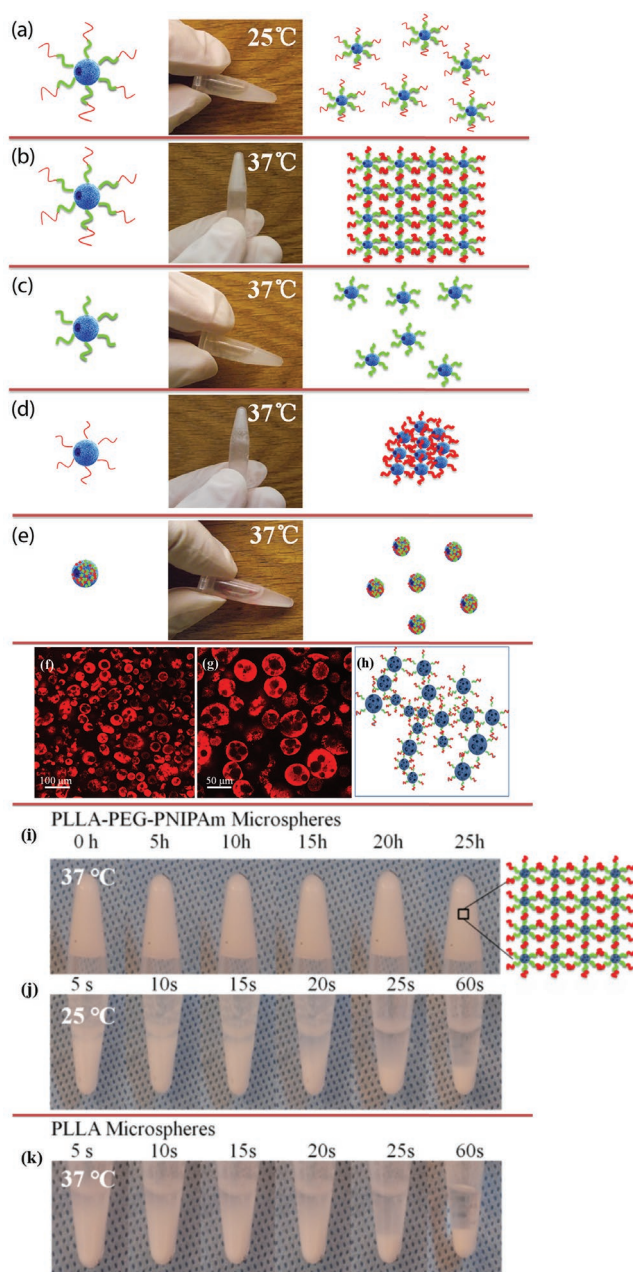


**Figure 4.** Thermoresponsive gelation of PLLA-PEG-PNIPAm NF-GMS: a) aqueous dispersions with 5 w/v % of PLLA-PEG-PNIPAm<sup>c</sup> (68/9/23 wt%) NF-GMS at 25 °C, b) PLLA-PEG-PNIPAm<sup>c</sup> (68/9/23 wt%) NF-GMS at 37 °C, c) PLLA-PEG (89/11 wt%) NF-HMS at 37 °C, d) PLLA-PNIPAm (73/27 wt%) NF-HMS at 37 °C, and e) PLLA-PEG-PNIPAm (52/14/34 wt%) random copolymer microspheres at 37 °C. Confocal fluorescence micrographs of hydrogels: f,g) 5 w/v % PLLA-PEG-PNIPAm<sup>c</sup> NF-GMS (60–90 μm) at 37 °C, the microspheres were stained by rhodamine-BSA, h) Schematic representation of the crosslinking of PLLA-PEG-PNIPAm<sup>c</sup> (68/9/23 wt%) NF-GMS inside the hydrogel at 37 °C. Stability of aqueous dispersions with 5 w/v % of i) PLLA-PEG-PNIPAm<sup>c</sup> (68/9/23 wt%) NF-GMS at 37 °C, j) PLLA-PEG-PNIPAm<sup>c</sup> (68/9/23 wt%) NF-GMS at 25 °C, and k) PLLA NF-HMS at 37 °C.

percentages of PLLA, PEG, and PNIPAm in the copolymer were about or higher than 68, 5, and 11 wt%, respectively, NF-GMS became nanofibrous and formed a free-standing hydrogel at body temperature.

## 2.6. NF-GMS Significantly Enhanced CM-Transplantation Mediated Heart Regeneration

To determine the important role of NF-GMS in supporting CM maintenance and function based on our hypothesis driven design, CMs were cultured with NF-GMS for 7 days *in vitro*. The open and hollow structure of NF-GMS facilitated CM incorporation, even distribution, and attachment to the NF-GMS. The gel formation of NF-GMS prevented CM leakage and allowed CM interactions. CMs in the gel retained the normal CM structure with the expression of cardiac troponin T (Figure S10, Supporting Information). Moreover, we also co-cultured CMs with collagen-I (the major ECM in heart and particularly after MI injury) or NF-GMS with 50 μM H<sub>2</sub>O<sub>2</sub> treatment to mimic *in vivo* MI injury. NF-GMS significantly increased cell survival after H<sub>2</sub>O<sub>2</sub> treatment compared to collagen-I by Western blot with Bcl-2 (anti-apoptosis marker) and Bax (pro-apoptosis marker) antibodies (Figure S11, Supporting Information). High-magnification images showed the cell-cell connections, suggesting cardiac tissue maturation and integration (Figure S12, Supporting Information). Importantly, CMs in the gel maintained the cardiac beating property (Video S1, Supporting Information).

To evaluate the long-term cell retention and *in vivo* engraftment of NF-GMS carried CMs, we transplanted hESC-derived CMs with NF-GMS.  $1 \times 10^7$  hESC-CMs mixed with NF-GMS at the number ratio of 30:1 were suspended in 100 μL PBS and injected into a rat heart after MI injury. 100 μL PBS, NF-GMS alone, and  $1 \times 10^7$  hESC-CMs suspended in 100 μL PBS without NF-GMS were injected as controls. The engraftment size of the transplanted hESC-CMs was assessed at day 28 after cell transplantation by immunofluorescence staining with human specific mitochondrial antibody (Hu-mito). In the CMs only group, CMs were found mainly in the infarct border zone and occasionally in the infarct zone (Figure 5A). In the CM+NF-GMS group, much larger and confluent CM grafts were identified in both the border zone and the infarct zone (Figure 5A,B). The graft volume was calculated using a published method<sup>[21]</sup> by combining the stained slides every 0.5 mm away from the apex to the base of the heart. The graft area in each slide was measured using ImageJ software. There was a tenfold higher graft size in the CM+NF-GMS group than that in the CM only group in infarcted rat heart (Figure 5A). The engraftment of CMs carried by NF-GMS was also detected using immunofluorescence staining against cTnT and anti-Hu-mito antibodies (Figure 5B, upper panel). Furthermore, abundant gap junctions formed among CMs in the transplanted areas as indicated by Connexin 43 staining (Figure 5B, lower panel as well as higher magnification images in Figure S12, Supporting Information), indicating that NF-GMS carried CM transplantation also promoted cell-cell integrations.

The long-term survival and integration of transplanted CMs would require adequate vascular network support in the engrafted areas. Therefore, we evaluated the vascular density in the infarction border zone and the remote zone (non-infarct zone) in the infarcted rat heart by staining with endothelial cell marker CD31. The number of vessel-like lumens was calculated to assess the vascular density 28 days after cell transplantation (Figure 5 C,D). Vascular density in the remote zone was greater

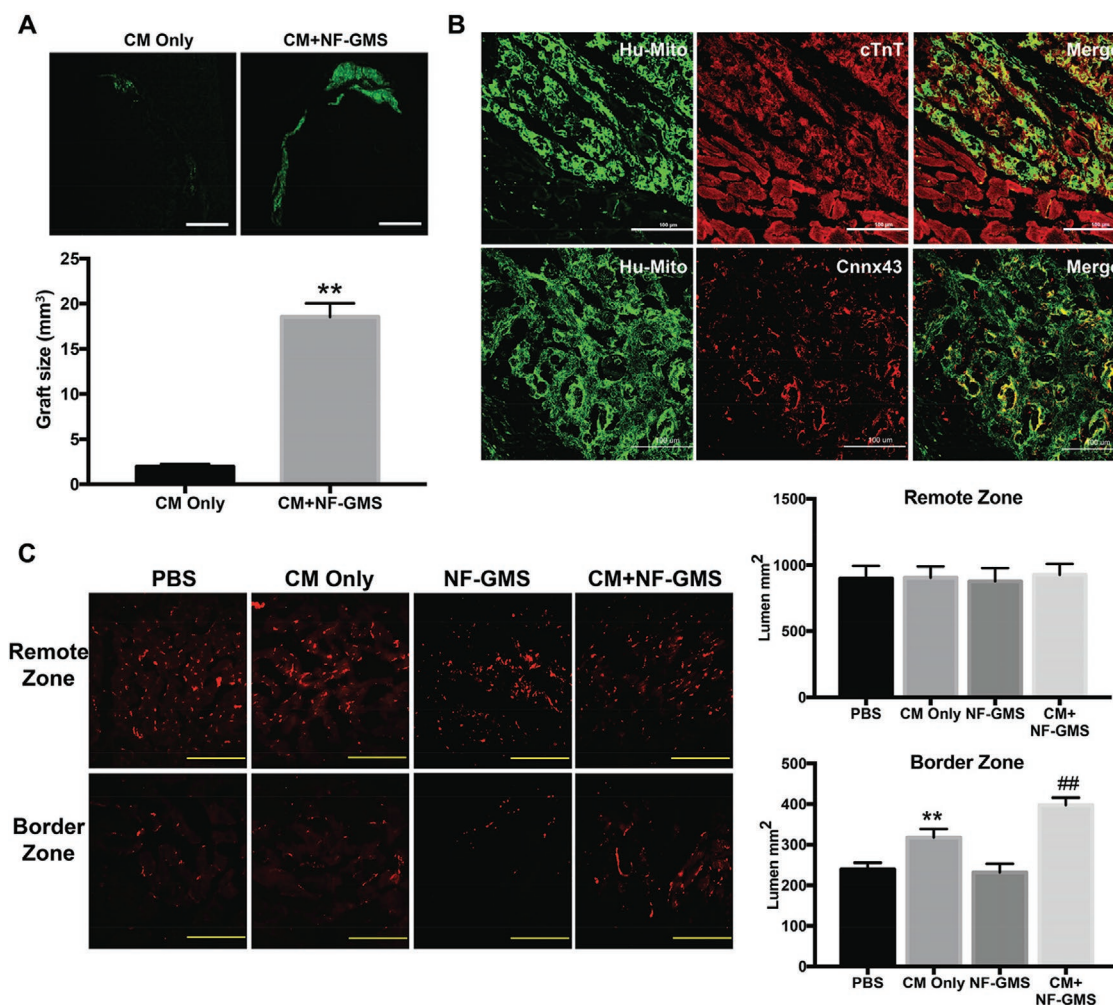


**Figure 5.** NF-GMS carried hESC-CM engraftment and angiogenesis. CM engraftment was illustrated by A) human specific antigen (Hu-mito) staining and quantitative analysis, and B) immunofluorescence staining against Hu-mito and cTnT. Rat I/R hearts were analyzed 4 weeks after transplantation.  $N = 9$ , \*\*,  $p < 0.01$ , compared with CM group. Much larger and confluent CM grafts were identified predominantly in both the border zone and the infarct zone in the CM+NF-GMS group, with a tenfold increase of engraftment over the CM only group. Furthermore, abundant gap junctions were formed as indicated by Connexin 43 staining (B, lower panel). C, D) Vessel-like lumens were quantified based on CD31 staining in the remote and border zones, respectively. Scale bars: 200  $\mu\text{m}$ ,  $n = 9$ , \*\*,  $p < 0.01$ , compared with PBS group; ##,  $p < 0.01$ , compared with CM group.

than in the border zone in all groups. No statistical significance of vascular density was observed in the remote zone among PBS, CM alone, NF-GMS alone, and CM+NF-GMS groups. A significantly higher vascular density was observed in the border zone of the CM+ NF-GMS group ( $398 \pm 18$ ) than those of the CM alone ( $318 \pm 21$ ), NF-GMS ( $231 \pm 22$ ) alone, and PBS ( $239 \pm 16$ ) groups ( $p < 0.01$ ). Thus, NF-GMS carried CM transplantation promoted revascularization in the border zone of the infarcted heart. The CD31/ $\alpha$ SMA double-staining showed stable vasculature 4 weeks after transplantation (Figure S13, Supporting Information).

To further evaluate heart regeneration by NF-GMS carried CM transplantation, Masson's trichrome staining was performed to identify blue scar tissue and red live tissue 28 days after transplantation (Figure 6). Live tissue was hardly observed in the infarcted areas of the PBS and NF-GMS only groups. Some clusters of live cells were found in the CM only group but were mainly near the border zone. In contrast, large clusters

of live cells were identified in both border zone and infarct zone in the CM+NF-GMS group, leading to a substantially thicker ventricle wall (see areas surrounded by the green line in Figure 6A). Strikingly, one month after NF-GMS carried CM injection, the infarct size in the CM+NF-GMS group was only 16% of LV, leading to a 58% reduction compared to PBS group, 50% reduction compared to NF-GMS only group, and a 43% reduction compared to CM only group ( $p < 0.01$ ). Furthermore, echocardiography was performed at day 6 to get the infarction baseline before cell transplantation. Myocardial infarction was confirmed in all groups with LVFS to be less than 35%. 28 days after cell transplantation, a significant increase in cardiac function was found in the CM+NF-GMS group with left ventricle ejection fractions (EF) = 54% and fractional shortening (FS) = 29%, indicating a striking functional recovery with 39% increase in EF and 46% increase in FS compared to PBS group ( $p < 0.01$ ). The cardiac function of CM+NF-GMS group was also significantly greater than that of CM only group with

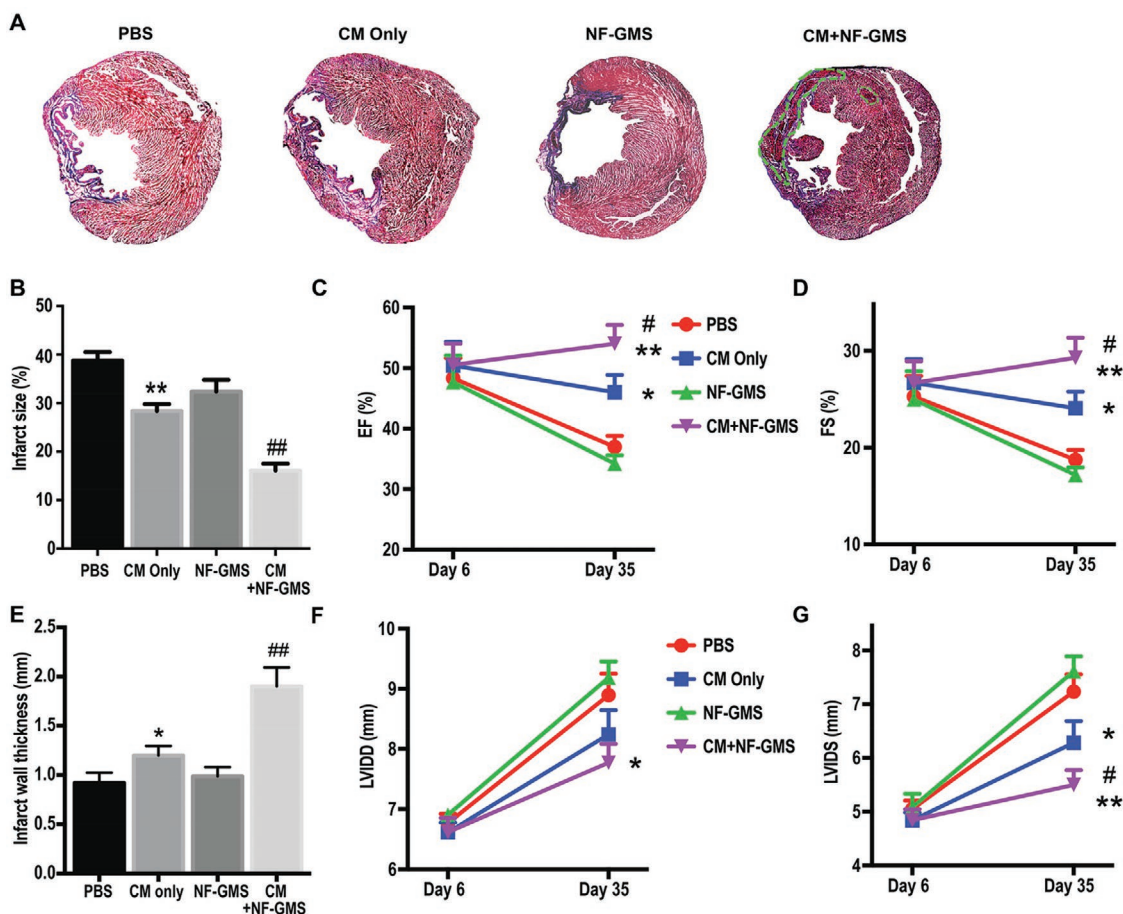


**Figure 6.** NF-GMS carried hESC-CM injection dramatically decreased infarct size and increased heart function as indicated by A) Masson trichrome staining, B) quantitative analysis, C) EF, and D) FS, E) wall thickness, F) LVIDD, and G) LVIDS evaluations. E) Rat MI hearts were analyzed 4 weeks after transplantation.  $N = 9$ , \*,  $p < 0.05$ , \*\*,  $p < 0.01$ , compared with PBS group; ##,  $p < 0.01$ , #,  $p < 0.05$ , compared with CM group. NF-GMS alone had little effect whereas CM+NF-GMS transplantation led to a 60% reduction in infarct size compared to PBS control.

a 17% higher EF and a 22% higher FS ( $p < 0.05$ ) (Figure 6). The high-resolution image of Masson's trichrome staining (Figure S14, Supporting Information) showed reduction in fibrosis (blue) in CM+NF-GMS group. CD68 staining showed modest immune cell infiltration (CD68+) in MI heart 4 weeks after cell transplantation, likely resulted from mainly I/R injury because there were no significant differences between PBS, NF-GMS only, CM only, and CM+NF-GMS groups (Figure S15, Supporting Information). Collectively, our studies showed that NF-GMS carried CM transplantation achieved the highest CM engraftment to date, substantially reduced infarct size, enhanced revascularization, and resulted in significant functional recovery compared to CM transplantation alone.

### 3. Discussion

In order to more comprehensively mimic ECM and obtain superb injectable cell carriers for heart regeneration after a heart attack, we successfully developed a new biodegradable tri-block PLLA-PEG-PNIPAm copolymer that self-assembles into novel nanofibrous microspheres NF-GMS, which in an

aqueous suspension are an injectable free-flowing liquid at room temperature and undergo thermally-responsive gelation after injection in vivo to reconstruct complex 3D wounds. The development of the NF-GMS represents several breakthroughs: 1) a route to synthesize PLLA-based tri-block copolymers with drastically different chemical and physical properties among the three blocks, resulting in a new biodegradable and biocompatible thermoresponsive polymer; 2) a new microcarrier that mimics the ECM in both nanofibrous feature and its hydrogel properties; 3) drastic increases in CM retention and engraftment, which have been the critical bottleneck of cardiac regeneration; 4) a substantial reduction of infarct size and a substantial recovery of cardiac function of an infarcted heart.

Pure PLLA has been previously fabricated into macroscopic 3D nanofibrous scaffolds using a novel phase-separation technique in our lab<sup>[22]</sup> for various tissue regeneration applications.<sup>[23]</sup> PLLA is the major component of the new tri-block copolymer and contributes to the microsphere body and nanofibrous structure. While various NF microspheres have been developed using star-shaped PLLA by our group,<sup>[24]</sup> those microspheres are discrete particles and unable to form the desired integrative hydrogels. While ATRP and ROP have



been used in combination to synthesize other types of triblock copolymers to form nanosized drug delivery particles,<sup>[25]</sup> none of them has been reported to form nanofibrous microparticles such as the NF-GMS in this work. By copolymerizing PLLA with PEG and PNIPAm using ATRP and ROP, we successfully synthesized PLLA-PEG-PNIPAm triblock copolymer for the first time, imparting hydrophilicity and temperature-triggered physical crosslinks to enable macroscale gel formation. However, chemical modification of PLLA is known to interfere with its fiber formation.<sup>[26]</sup> More challengingly, due to the limited contact area between spheres, there is a sharp increase in difficulty to build strong interactions between spheres to construct a stable 3D network for hydrogel formation when the diameter of spheres is large, such as on the micrometer scale in this study. By examining the competing requirements for nanofiber and gel formation, structural requirements of NF-GMS formation are revealed. Macroscopic hydrogel of the NF-GMS is developed and its modulus can be tuned over several orders of magnitude. In addition, the PLLA-PEG-PNIPAm NF-GMS degrade in a desired time duration for heart regeneration. Furthermore, NF-GMS carried CM delivery leads to remarkably efficient CM engraftment and significantly improves heart function after infarction in an acute rat MI model. Nanofibrous structure is known to advantageously support various tissue regeneration,<sup>[20b]</sup> gel properties can affect cell behavior<sup>[27]</sup> and could have protective effect on injured heart.<sup>[28]</sup>

The superior engraftment efficiency of NF-GMS carried cell transplantation appears due to the two most important ECM-mimicking characteristics of this advanced CM carrier: the nanofiber feature and the gelling property. Consistent with this notion, we previously showed porous and nanofibrous scaffolds to enhance cardiac differentiation over control non-nanofibrous scaffolds.<sup>[29]</sup> CM delivery using NF microspheres without gelling property resulted in significantly lower enhancement in CM engraftment (3.4-fold enhancement over CM only, unpublished data) compared to the approximately tenfold CM engraftment increase using the NF-GMS hydrogel. Various hydrogels were reported to improve CM retention or protection,<sup>[28,30]</sup> but their improvements were not at the same level as NF-GMS in this work. For example, we previously showed that a fibrin gel without the nanofibrous microspheres had significantly lower enhancement in CM engraftment (about 2.3-fold over CM suspension alone)<sup>[31]</sup> compared to the tenfold CM engraftment enhancement of the NF-GMS hydrogel. NF-GMS achieved the highest CM engraftment enhancement among all carriers reported this far.

There was no statistically significant difference in cardiac function between NF-GMS alone and PBS alone control groups without cells, suggesting that the NF-GMS did not mechanically contribute to the cardiac function of the infarcted heart. However, when CMs were transplanted, NF-GMS enhanced the CM engraftment and improved cardiac function versus all control groups. The temperature induced NF-GMS hydrogel (at 37 °C) has low modulus, which may not enhance cardiac function mechanically by itself. However, the low modulus may facilitate cardiac differentiation.<sup>[32]</sup> The CM+NF-GMS group enhanced cardiac tissue regeneration (reduced infarct size) over CM alone or NF-GMS alone groups. Importantly, CM+NF-GMS group showed the best functional properties among all groups after 35 days of implantation.

Collectively, the novel NF-GMS self-assembled from the new triblock copolymer, integrating the ECM-mimicking NF architecture with a temperature-responsive in situ gel-forming property, are a highly promising microcarrier for heart regeneration and likely for many other types of tissue regeneration.

## 4. Experimental Section

**PEG macroinitiator (HO-PEG-Br) synthesis (reaction 1):** A typical procedure to synthesize HO-PEG-Br is as follows: Dry THF (25 mL), dry polyethylene glycol (PEG) (6.68 mmol) and dry triethylamine (TEA) (20 mmol, 1.5 mL) were placed in a 250 mL round-bottom flask, kept under a nitrogen atmosphere. Within 1 h, BIBB (6.68 mmol, 0.83 mL) was slowly added via a dropping funnel. After the addition was complete, the mixture was stirred at room temperature overnight. The precipitated salts were filtered off, and the filtrate was evaporated in vacuum. Then 1 M hydrochloric acid (HCl) (30 mL) was added and the mixture was extracted with dichloromethane (3 × 20 mL). The combined organic layers were washed three times with water (50 mL) to remove salt. The organic layer was dried over anhydrous Na<sub>2</sub>SO<sub>4</sub> overnight. After removal of the solvent, the polymer was precipitated into cold ethyl ether and collected by filtration. The resultant white powder was dried in vacuum for 24 h to give HO-PEG-Br.

**PEG-PNIPAm (reaction 2: ATRP):** A typical procedure to synthesize PEG-PNIPAm ( $M_n = 5371$ ) is as follows: PEG macroinitiator ( $M_n = 1551$ ) (0.6 mmol, 1 g), NIPAm (26.5 mmol, 3 g), and CuCl (0.170 mmol, 0.0168 g) were placed in a 250 mL round-bottom flask under nitrogen protection and sealed with rubber septum stoppers. Milli-Q water (20 mL) and Me<sub>6</sub>TREN (0.174 mmol, 0.04 g) were placed in a Schlenk tube and purged with N<sub>2</sub> gas for 40 min. The solution was transferred to the round-bottom flask using a syringe under nitrogen protection. The reaction mixture was then stirred under nitrogen atmosphere for 24 h. The reaction was then stopped by opening the vessel to air. The reaction mixture was precipitated into ethyl ether, filtered, and dried. The resulting solid was then dissolved in H<sub>2</sub>O and dialyzed (MW cut-off 3.5 kDa) against de-ionized water for 3 days to remove unreacted PEG-macroinitiator. The mixture was then lyophilized for 3 days to give PEG-PNIPAm copolymer.

**PLLA-PEG-PNIPAm (reaction 3: ROP):** A typical procedure to synthesize PLLA-PEG-PNIPAm<sup>c</sup> is as follows: Dry THF (10 mL), L-lactide (139 mmol, 2 g), PEG-PNIPAm ( $M_n = 5371$ ) (0.0559 mmol, 0.3 g) and Sn(Oct)<sub>2</sub> (0.4 mmol, 0.162 g) were mixed in a 50 mL round-bottom flask with stirring and nitrogen purging. The mixture was heated to 80 °C under nitrogen protection for complete melting. The polymerization was carried out at 80 °C under nitrogen protection for 24 h. The crude product was dissolved in 20 mL chloroform, precipitated in 100 mL cold methanol, and then vacuum dried.

Fabrication of microspheres. PLLA-PEG-PNIPAm copolymer was dissolved in THF at 60 °C with a concentration of 2.0% (wt/v). Under rigorous mechanical stirring (speed 7, MAXIMA, Fisher Scientific), glycerol (60 °C) with three times the volume of the PLLA-PEG-PNIPAm copolymer solution was gradually added into the PLLA-PEG-PNIPAm copolymer solution. Stirring was continued for 5 min afterwards. The mixture was then quickly poured into liquid nitrogen. After 10 min, a water ice mixture (1000 mL) was added for solvent exchange for 24 h. The spheres were sieved and washed with an excessive amount of distilled water six times to remove glycerol residue. The spheres were then lyophilized for 3 days.

**Differentiation and Characterization of Human Embryonic Stem Cell Derived Cardiomyocytes (hESC-CMs):** hESCs (H7 cell line) were differentiated into cardiomyocytes (CMs) using chemically defined culture similar to that described in literature.<sup>[33]</sup> Full confluent single layer hESCs were cultured in CDM3 medium to induce CM differentiation. Lactate instead of glucose medium was applied to purify CMs from day 12 to day 18.<sup>[33b,34]</sup> At day 20, the derived CMs were digested by trypsin for flow cytometry assay or subsequent transplantation. Typically, 90%

or more resulting cells were cTnT + CMs using the above described differentiation process.

**SEM and Immunofluorescence Assay of Co-Cultured CMs and NF-GMS:** Five million CMs mixed with NF-GMS at the ratio of 30:1 were co-cultured in 35 mm petri dishes (Falcon) with CDM3 medium for 7 days. For scanning electron microscope (SEM) assay, the samples were collected and fixed in 2.5% glutaraldehyde and 2% paraformaldehyde overnight at 4 °C. After post-fixation in 1% osmium tetroxide at room temperature for 1 h, samples were dehydrated in increasing concentrations of ethanol and dried with hexamethyldisilazane. NF-GMS only or the CM+NF-GMS samples were sputter-coated with gold and observed under an SEM (Phillips XL30 FEG).

For immunofluorescence staining, samples were fixed with 4% paraformaldehyde at room temperature for 20 min, frozen in Tissue-Plus O.C.T Compound (Fisher Scientific), and cryosectioned into 7 μm sections. Slide sections were permeabilized with 0.3% Triton X-100 for 15 min at room temperature, blocked with 5% horse serum in DPBS-T for 1 h at room temperature and incubated with primary antibodies against cTnT (ab45932, Abcam) at 4 °C overnight in 2% horse serum. Sections were then washed 3 times with PBS for 15 min each time, incubated with Alexa Fluor 488-conjugated secondary antibodies (Thermo Fisher Scientific) in 2% horse serum in DPBS-T for 1 h at room temperature, washed with PBS for 3 times and 15 min each time, then stained with DAPI, and images were obtained by fluorescence microscope (Olympus, Japan).

**Generation of Myocardial Infarction Rats and Cell Transplantation:** All animal experiments were approved by the Institutional Animal Care and Use Committee of the University of Michigan. 8 week-old (190–210 g) Female Sprague Dawley rats were purchased from ENVIGO. Myocardial infarction was induced by ischemia reperfusion (I/R) surgery.<sup>[8b,35]</sup> In brief, the animal heart was exposed by an open thoracotomy and the left anterior descending artery was ligated with 6–0 sutures for 60 min and reperused by loosening the suture. Animals were randomly divided into 4 groups: PBS control, CM only, NF-GMS only, and CM+NF-GMS group. Cell transplantation was carried out following the literature<sup>[8b,35b]</sup> with minor modifications. Briefly, 7 days after I/R (which is within the reported best time window of 4 day to 2 weeks after MI for cardiomyocyte transplantation<sup>[7a,8c,36]</sup>), animals underwent a second thoracotomy and 100 μL PBS or cell suspension containing  $1 \times 10^7$  hESC-CMs were injected at 5 sites into the border zone of the infarction. In the CM+NF-GMS group, CMs and NF-GMS at the ratio of 30:1 were mixed before injection. Immunosuppressor cyclosporine A was subcutaneously administered 10 mg kg<sup>-1</sup> day<sup>-1</sup> from 2 days before cell transplantation until animals were sacrificed.

**Histology and Immunohistochemistry:** Hearts were fixed in 4% paraformaldehyde, frozen in Tissue-Plus O.C.T Compound (Fisher Scientific), and cryosectioned into 7 μm sections for immunohistochemistry and histological analyses. For immunofluorescence staining, the procedure was the same as for those in vitro CM+NF-GMS samples described above. Staining with primary antibodies against human mitochondrion (MAB1273, EMD Millipore) was performed to identify the transplanted CMs in rat heart. Staining with cTnT (ab45932, Abcam) and Cnnx43 (sc-9059, Santa Cruz Biotechnology) antibodies was performed to characterize CM structure and cell-cell connection. After staining, slides were mounted using ProLong Diamond Antifade Mountant (P36970, Thermo Fisher Scientific) and imaged using a Nikon A1 Confocal Laser Microscope. Staining with anti-CD31 (sc-1506, Santa Cruz Biotechnology) antibody was used to investigate vascular density. In addition, Masson's trichrome staining was performed to calculate the infarct size in rat hearts.

**Assessment of Cardiac Function:** Echocardiography was performed at day 6 and day 35 to evaluate cardiac function. Left ventricular internal diameter at end-diastole (LVIDD) and left ventricular internal diameter at end-systole (LVIDS) were measured using a Vevo 2100 system.<sup>[37]</sup> Left ventricle ejection fractions (EF) and fractional shortening (FS) were calculated using the equations: EF (%) = (LVIDD<sup>3</sup>–LVIDS<sup>3</sup>)/LVIDD<sup>3</sup> × 100%; and FS (%) = (LVIDD–LVIDS)/LVIDD × 100%. All echocardiography measurement and analysis were performed by a

single-blinded investigator in Frankel Cardiovascular Center of University of Michigan.

**Statistical Analysis:** The data are presented as the mean ± SEM. All results were assessed using Graphpad Prism software. Statistical analyses were performed using a Student's *t*-test or a one-way ANOVA test. A *p* value < 0.05 was considered statistically significant.

## Supporting Information

Supporting Information is available from the Wiley Online Library or from the author.

## Acknowledgements

The authors would like to acknowledge the financial support from the NIH (HL114038, HL136231, HL109054, and HL139735). The authors would like to thank Dr. Mario Fabiilli for kindly making the Multisizer 4 Coulter Counter available.

## Conflict of Interest

The authors declare no conflict of interest.

## Author Contributions

C.Z., S.T., and Q.L. contributed equally to this project. C.Z. carried out the polymer synthesis, nanofibrous gelling microsphere fabrication, their structural, microscopic, thermal, mechanical, and degradation characterization. S.T. and Q.L. carried out the cellular, animal, biochemical, surgical, histological, and functional studies. K.X. measured the NF-GMS size distribution. I.L. helped with the cardiac differentiation of ESCs. Z.W. was responsible for cells and animal studies. P.X.M. was responsible for the overall project design, execution, and manuscript organization and finalization. P.X.M. specifically oversaw the polymer synthesis, carrier fabrication, and tissue engineering studies. All authors contributed to the experimental planning, data analysis, and interpretation.

## Keywords

block copolymers, cell transplantation, heart regeneration, hydrogels, nanofibers

Received: January 27, 2020  
Published online: March 20, 2020

- [1] E. J. Benjamin, M. J. Blaha, S. E. Chiuve, M. Cushman, S. R. Das, R. Deo, S. D. de Ferranti, J. Floyd, M. Fornage, C. Gillespie, C. R. Isasi, M. C. Jimenez, L. C. Jordan, S. E. Judd, D. Lackland, J. H. Lichtman, L. Lisabeth, S. Liu, C. T. Longenecker, R. H. Mackey, K. Matsushita, D. Mozaffarian, M. E. Mussolino, K. Nasir, R. W. Neumar, L. Palaniappan, D. K. Pandey, R. R. Thiagarajan, M. J. Reeves, M. Ritchey, et al., *Circulation* **2017**, *135*, e146.
- [2] Z. Lin, W. T. Pu, *Sci. Transl. Med.* **2014**, *6*, 239rv1.
- [3] D. Mozaffarian, E. J. Benjamin, A. S. Go, D. K. Arnett, M. J. Blaha, M. Cushman, S. R. Das, S. de Ferranti, J. P. Despres, H. J. Fullerton, V. J. Howard, M. D. Huffman, C. R. Isasi, M. C. Jimenez, S. E. Judd, B. M. Kissela, J. H. Lichtman, L. D. Lisabeth, S. Liu, R. H. Mackey,

- D. J. Magid, D. K. McGuire, E. R. Mohler III, C. S. Moy, P. Muntner, M. E. Mussolino, K. Nasir, R. W. Neumar, G. Nichol, L. Palaniappan, et al., *Circulation* **2016**, *133*, 447.
- [4] a) A. P. Beltrami, K. Urbanek, J. Kajstura, S. M. Yan, N. Finato, R. Bussani, B. Nadal-Ginard, F. Silvestri, A. Leri, C. A. Beltrami, P. Anversa, *N. Engl. J. Med.* **2001**, *344*, 1750; b) S. E. Senyo, M. L. Steinhauser, C. L. Pizzimenti, V. K. Yang, L. Cai, M. Wang, T. D. Wu, J. L. Guerquin-Kern, C. P. Lechene, R. T. Lee, *Nature* **2013**, *493*, 433; c) E. Tzahor, K. D. Poss, *Science* **2017**, *356*, 1035.
- [5] G. Kaushik, A. Spenlehauer, A. O. Sessions, A. S. Trujillo, A. Fuhrmann, Z. Fu, V. Venkatraman, D. Pohl, J. Tuler, M. Wang, E. G. Lakatta, K. Ocorr, R. Bodmer, S. I. Bernstein, J. E. V. Eyk, A. Cammarato, A. J. Engler, *Sci. Transl. Med.* **2015**, *7*, 292ra99.
- [6] a) J. H. van Berlo, O. Kanisicak, M. Maillet, R. J. Vagnozzi, J. Karch, S. C. Lin, R. C. Middleton, E. Marban, J. D. Molkentin, *Nature* **2014**, *509*, 337; b) N. Sultana, L. Zhang, J. Yan, J. Chen, W. Cai, S. Razzaque, D. Jeong, W. Sheng, L. Bu, M. Xu, G. Y. Huang, R. J. Hajjar, B. Zhou, A. Moon, C. L. Cai, *Nat. Commun.* **2015**, *6*, 8701; c) B. Zhou, S. M. Wu, *Circ. Res.* **2018**, *123*, 9; d) K. Kretzschmar, Y. Post, M. Bannier-Helaouet, A. Mattiotti, J. Drost, E. Basak, V. S. W. Li, M. van den Born, Q. D. Gunst, D. Versteeg, L. Kooijman, S. van der Elst, J. H. van Es, E. van Rooij, M. J. B. van den Hoff, H. Clevers, *Proc. Natl. Acad. Sci. USA* **2018**, *115*, E12245.
- [7] a) Y. Shiba, S. Fernandes, W. Z. Zhu, D. Filice, V. Muskheli, J. Kim, N. J. Palpant, J. Gantz, K. W. Moyes, H. Reinecke, B. V. Biber, T. Dardas, J. L. Mignone, A. Izawa, R. Hanna, M. Viswanathan, J. D. Gold, M. I. Kotlikoff, N. Sarvazyan, M. W. Kay, C. E. Murry, M. A. Laflamme, *Nature* **2012**, *489*, 322; b) F. Weinberger, K. Breckwoldt, S. Pecha, A. Kelly, B. Geertz, J. Starbatty, T. Yorgan, K. H. Cheng, K. Lessmann, T. Stolen, M. Scherrer-Crosbie, G. Smith, H. Reichenspurner, A. Hansen, T. Eschenhagen, *Sci. Transl. Med.* **2016**, *8*, 363ra148.
- [8] a) E. Elhami, B. Dietz, B. Xiang, J. Deng, F. Wang, C. Chi, A. L. Goertzen, S. Mzengeza, D. Freed, R. C. Arora, G. Tian, *EJNMMI Res.* **2013**, *3*, 72; b) M. A. Laflamme, K. Y. Chen, A. V. Naumova, V. Muskheli, J. A. Fugate, S. K. Dupras, H. Reinecke, C. Xu, M. Hassanipour, S. Police, C. O'Sullivan, L. Collins, Y. Chen, E. Minami, E. A. Gill, S. Ueno, C. Yuan, J. Gold, C. E. Murry, *Nat. Biotechnol.* **2007**, *25*, 1015; c) S. Fernandes, A. V. Naumova, W. Z. Zhu, M. A. Laflamme, J. Gold, C. E. Murry, *J. Mol. Cell. Cardiol.* **2010**, *49*, 941.
- [9] a) A. Aicher, W. Brenner, M. Zuhayra, C. Badorff, S. Massoudi, B. Assmus, T. Eckey, E. Henze, A. M. Zeiher, S. Dimmeler, *Circulation* **2003**, *107*, 2134; b) D. Hou, E. A. Youssef, T. J. Brinton, P. Zhang, P. Rogers, E. T. Price, A. C. Yeung, B. H. Johnstone, P. G. Yock, K. L. March, *Circulation* **2005**, *112*, 1150.
- [10] a) R. Dong, X. Zhao, B. Guo, P. X. Ma, *ACS Appl. Mater. Interfaces* **2016**, *8*, 17138; b) B. Pena, M. Laughter, S. Jett, T. J. Rowland, M. R. G. Taylor, L. Mestroni, D. Park, *Macromol. Biosci.* **2018**, *18*, 1800079; c) F. Weinberger, I. Mannhardt, T. Eschenhagen, *Circ. Res.* **2017**, *120*, 1487.
- [11] J. J. Chong, X. Yang, C. W. Don, E. Minami, Y. W. Liu, J. J. Weyers, W. M. Mahoney, B. V. Biber, S. M. Cook, N. J. Palpant, J. A. Gantz, J. A. Fugate, V. Muskheli, G. M. Gough, K. W. Vogel, C. A. Astley, C. E. Hotchkiss, A. Baldessari, L. Pabon, H. Reinecke, E. A. Gill, V. Nelson, H. P. Kiem, M. A. Laflamme, C. E. Murry, *Nature* **2014**, *510*, 273.
- [12] a) L. Ye, Y. H. Chang, Q. Xiong, P. Zhang, L. Zhang, P. Somasundaram, M. Lepley, C. Swingen, L. Su, J. S. Wendel, J. Guo, A. Jang, D. Rosenbush, L. Greder, J. R. Dutton, J. Zhang, T. J. Kamp, D. S. Kaufman, Y. Ge, J. Zhang, *Cell Stem Cell* **2014**, *15*, 750; b) J. Tang, J. Wang, K. Huang, Y. Ye, T. Su, L. Qiao, M. T. Hensley, T. G. Caranasos, J. Zhang, Z. Gu, K. Cheng, *Sci. Adv.* **2018**, *4*, eaat9365.
- [13] B. P. Purcell, D. Lobb, M. B. Charati, S. M. Dorsey, R. J. Wade, K. N. Zellars, H. Doviak, S. Pettaway, C. B. Logdon, J. A. Shuman, P. D. Freels, J. H. Gorman III, R. C. Gorman, F. G. Spinale, J. A. Burdick, *Nat. Mater.* **2014**, *13*, 653.
- [14] F. F. Wolf, N. Friedemann, H. Frey, *Macromolecules* **2009**, *42*, 5622.
- [15] a) M. Semsarilar, S. Perrier, *Nat. Chem.* **2010**, *2*, 811; b) A. Gregory, M. H. Stenzel, *Prog. Polym. Sci.* **2012**, *37*, 38.
- [16] K. Matyjaszewski, N. V. Tsarevsky, *Nat. Chem.* **2009**, *1*, 276.
- [17] W. Xiu-fang, J.-l. Lan, L. Ying, P. Pihui, C. Zhi-Qi, X. Shou-ping, Z. Li-juan, Q. Yu, *Polym. Int.* **2014**, *63*, 1238.
- [18] a) N. E. Kamber, W. Jeong, R. M. Waymouth, R. C. Pratt, B. G. G. Lohmeijer, J. L. Hedrick, *Chem. Rev.* **2007**, *107*, 5813; b) O. Dechy-Cabaret, B. Martin-Vaca, D. Bourissou, *Chem. Rev.* **2004**, *104*, 6147.
- [19] C. Zhao, L. Li, J. Zheng, *Langmuir* **2010**, *26*, 17375.
- [20] a) R. Langer, J. Vacanti, *Science* **1993**, *260*, 920; b) P. X. Ma, *Adv. Drug Delivery Rev.* **2008**, *60*, 184.
- [21] K. Tambara, G. U. Premaratne, G. Sakaguchi, N. Kanemitsu, X. Lin, H. Nakajima, Y. Sakakibara, Y. Kimura, M. Yamamoto, Y. Tabata, T. Ikeda, M. Komeda, *Circulation* **2005**, *112*, 1129.
- [22] a) P. X. Ma, R. Zhang, *J. Biomed. Mater. Res.* **1999**, *46*, 60; b) H. Ma, J. Hu, P. X. Ma, *Adv. Funct. Mater.* **2010**, *20*, 2833.
- [23] G. Wei, P. X. Ma, *Adv. Funct. Mater.* **2008**, *18*, 3566.
- [24] a) X. Liu, X. Jin, P. X. Ma, *Nat. Mater.* **2011**, *10*, 398; b) Z. Zhang, M. J. Gupte, X. Jin, P. X. Ma, *Adv. Funct. Mater.* **2015**, *25*, 350; c) Z. Zhang, R. L. Marson, Z. Ge, S. C. Glotzer, P. X. Ma, *Adv. Mater.* **2015**, *27*, 3947.
- [25] J. Chen, M. Liu, H. Gong, Y. Huang, C. Chen, *J. Phys. Chem. B* **2011**, *115*, 14947.
- [26] X. Liu, P. X. Ma, *Biomaterials* **2010**, *31*, 259.
- [27] J. H. Wen, L. G. Vincent, A. Fuhrmann, Y. S. Choi, K. C. Hribar, H. Taylor-Weiner, S. Chen, A. J. Engler, *Nat. Mater.* **2014**, *13*, 979.
- [28] J. L. Ifkovits, E. Tous, M. Minakawa, M. Morita, J. D. Robb, K. J. Koomalsingh, J. H. Gorman III, R. C. Gorman, J. A. Burdick, *Proc. Natl. Acad. Sci. USA* **2010**, *107*, 11507.
- [29] Q. Liu, S. Tian, C. Zhao, X. Chen, I. Lei, Z. Wang, P. X. Ma, *Acta Biomater.* **2015**, *26*, 105.
- [30] a) T. Kofidis, J. L. de Bruin, G. Hoyt, D. R. Lebl, M. Tanaka, T. Yamane, C. P. Chang, R. C. Robbins, *J. Thorac. Cardiovasc. Surg.* **2004**, *128*, 571; b) K. L. Christman, H. H. Fok, R. E. Sievers, Q. Fang, R. J. Lee, *Tissue Eng.* **2004**, *10*, 403; c) C. P. Jackman, A. L. Carlson, N. Bursac, *Biomaterials* **2016**, *111*, 66; d) Z. Li, X. Guo, S. Matsushita, J. Guan, *Biomaterials* **2011**, *32*, 3220; e) M. Tokunaga, M. L. Liu, T. Nagai, K. Iwanaga, K. Matsuura, T. Takahashi, M. Kanda, N. Kondo, P. Wang, A. T. Naito, I. Komuro, *J. Mol. Cell. Cardiol.* **2010**, *49*, 972; f) T. Yoshizumi, Y. Zhu, H. Jiang, A. D'Amore, H. Sakaguchi, J. Tchao, K. Tobita, W. R. Wagner, *Biomaterials* **2016**, *83*, 182; g) H. Wang, Z. Liu, D. Li, X. Guo, F. K. Kasper, C. Duan, J. Zhou, A. G. Mikos, C. Wang, *J. Cell. Mol. Med.* **2012**, *16*, 1310.
- [31] Y. Li, S. Tian, I. Lei, L. Liu, P. X. Ma, Z. Wang, *Am. J. Transl. Res.* **2017**, *9*, 1530.
- [32] A. J. Engler, S. Sen, H. L. Sweeney, D. E. Discher, *Cell* **2006**, *126*, 677.
- [33] a) X. Lian, J. Zhang, S. M. Azarin, K. Zhu, L. B. Hazeltine, X. Bao, C. Hsiao, T. J. Kamp, S. P. Palecek, *Nat. Protoc.* **2013**, *8*, 162; b) P. W. Burridge, E. Matsa, P. Shukla, Z. C. Lin, J. M. Churko, A. D. Ebert, F. Lan, S. Diecke, B. Huber, N. M. Mordwinkin, J. R. Plews, O. J. Aibilez, B. Cui, J. D. Gold, J. C. Wu, *Nat. Methods* **2014**, *11*, 855.
- [34] S. Tohyama, F. Hattori, M. Sano, T. Hishiki, Y. Nagahata, T. Matsuura, H. Hashimoto, T. Suzuki, H. Yamashita, Y. Satoh, T. Egashira, T. Seki, N. Muraoka, H. Yamakawa, Y. Ohgino, T. Tanaka, M. Yoichi, S. Yuasa, M. Murata, M. Suematsu, K. Fukuda, *Cell Stem Cell* **2013**, *12*, 127.
- [35] a) S. Tian, I. Lei, W. Gao, L. Liu, Y. Guo, J. Creech, T. J. Herron, S. Xian, P. X. Ma, Y. Eugene Chen, Y. Li, H. B. Alam, Z. Wang,

- EBioMedicine* **2019**, *39*, 83; b) S. Fernandes, J. J. Chong, S. L. Paige, M. Iwata, B. Torok-Storb, G. Keller, H. Reinecke, C. E. Murry, *Stem Cell Rep.* **2015**, *5*, 753.
- [36] J. H. Traverse, T. D. Henry, C. J. Pepine, J. T. Willerson, D. X. Zhao, S. G. Ellis, J. R. Forder, R. D. Anderson, A. K. Hatzopoulos, M. S. Penn, E. C. Perin, J. Chambers, K. W. Baran, G. Raveendran, C. Lambert, A. Lerman, D. I. Simon, D. E. Vaughan, D. Lai, A. P. Gee, D. A. Taylor, C. R. Cogle, J. D. Thomas, R. E. Olson, S. Bowman, J. Francescon, C. Geither, E. Handberg, C. Kappenman, L. Westbrook, et al., *JAMA, J. Am. Med. Assoc.* **2012**, *308*, 2380.
- [37] A. Bhan, A. Sirker, J. Zhang, A. Protti, N. Catibog, W. Driver, R. Botnar, M. J. Monaghan, A. M. Shah, *Am. J. Physiol.: Heart Circ. Physiol.* **2014**, *306*, H1371.